CHEMISTRY OF MATERIALS

Perspective

pubs.acs.org/cm

Oxygen Evolution Reaction Electrocatalysis on Transition Metal Oxides and (Oxy)hydroxides: Activity Trends and Design Principles†

Michaela S. Burke, Lisa J. Enman, Adam S. Batchellor, Shihui Zou, and Shannon W. Boettcher*

Department of Chemistry and Biochemistry, University of Oregon, Eugene, Oregon 97403, United States

ABSTRACT: Poor oxygen evolution reaction (OER) catalysis limits the efficiency of H_2 production from water electrolysis and photoelectrolysis routes to large-scale energy storage. Despite nearly a century of research, the factors governing the activity of OER catalysts are not well understood. In this Perspective, we discuss recent advances in understanding the OER in alkaline media for earth-abundant, first-row, transition-metal oxides and (oxy)hydroxides. We argue that the most-relevant structures for study are thermodynamically stable (oxy)hydroxides and not crystalline oxides. We discuss thin-film electrochemical microbalance techniques to accurately quantify intrinsic activity and in situ conductivity measurements to identify materials limited by electronic transport. We highlight the dramatic effect that Fe cations—added either intentionally or unintentionally from ubiquitous electrolyte impurities—have on the activity of common OER catalysts. We find new activity trends across the first-row transition metals, opposite of the established ones, and propose a new view of OER on mixed-metal (oxy)hydroxides that illustrates possible design principles and applications.

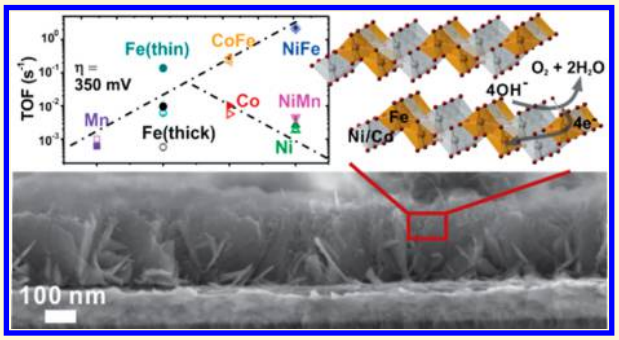

1.0. INTRODUCTION

The electrolysis or photoelectrolysis of water to generate oxygen and hydrogen gas could provide a scalable mechanism to store intermittent renewable energy needed to power a sustainable civilization. The hydrogen gas, an energy dense chemical, could later be used to generate electricity in a fuel cell or burned directly like natural gas.[1−5] Hydrogen is also already an important feedstock for the chemical industry in processes such as petroleum refining, Fischer−Tropsch synthesis of hydrocarbons, and the Haber−Bosch generation of ammonia.[6] Most hydrogen is now produced by steam-reforming of fossil fuels, with the greenhouse gas CO_2 formed as a byproduct.[2,5,6] Hydrogen produced by water electrolysis (i.e., water splitting) could, in principle, be CO_2 emission-free if the electricity was derived from renewables like wind or solar, but it must have increased efficiency and decreased costs to compete with fossil hydrogen sources.[2,5,6] The efficiency of electrolyzer systems is limited, in part, by the kinetic overpotential losses associated with driving the oxygen evolution reaction (OER) at the anode in both acidic ($2H_2O \rightarrow O_2 + 4H^+ + 4e^-$) and basic ($4OH^- \rightarrow O_2 + 2H_2O + 4e^-$) environments.[1,3,7,8] Solar water splitting further provides for the ability to integrate photovoltaic (energy conversion) and electrolyzer (energy storage) functionality into a single device, which could further lower hydrogen production costs relative to separate photovoltaic and electrolyzer systems.[1,3,4] These applications provide motivation for understanding materials that catalyze the OER in order to inform catalyst design efforts.

Electrolyzers have been commercially available for more than a century.[2,9,10] Traditional alkaline systems are the most common. They typically use nickel/stainless-steel mesh electrodes (which, at the anode, likely form Ni−Fe oxyhydroxide OER catalysts as discussed below). These electrodes are active and stable in the hot (~80 °C) concentrated aq. KOH or NaOH and typically operate at current densities of 100−500 mA cm^{-2}.[9,11,12] In the last few decades proton-exchange membrane (PEM) electrolysis technology has captured market share. PEM cells feature higher current densities (~2 A cm^{-2}), gas-impermeable membranes that allow for large differential pressures, the ability to run using neutral water as the feed source, and high purity hydrogen output.[2,10,13] The highly acidic conditions next to the membrane (e.g., Nafion), however, require the use of precious-metal catalysts, e.g., IrO_2 for the OER and Pt for hydrogen evolution.[2,10,13] While currently the catalyst cost is not a major factor in the total cost of the PEM electrolysis system, at a large scale, earth-abundant catalysts, which are only stable in neutral-to-alkaline conditions, will be necessary. Therefore, alkaline-exchange membrane (AEM) electrolyzers[14] with performance equal to, or better than, the acidic PEM systems would be attractive. One important challenge that we will not discuss here but that needs to be addressed is the design of anion exchange membranes with good stability and ionic conductivities.[9,11,15]

In order to design better OER catalysts it is useful to understand how they function, starting with measuring and

†This Perspective is part of the *Up-and-Coming* series.

Received: August 13, 2015
Published: October 14, 2015

DOI: 10.1021/acs.chemmater.5b03148
Chem. Mater. 2015, 27, 7549−7558

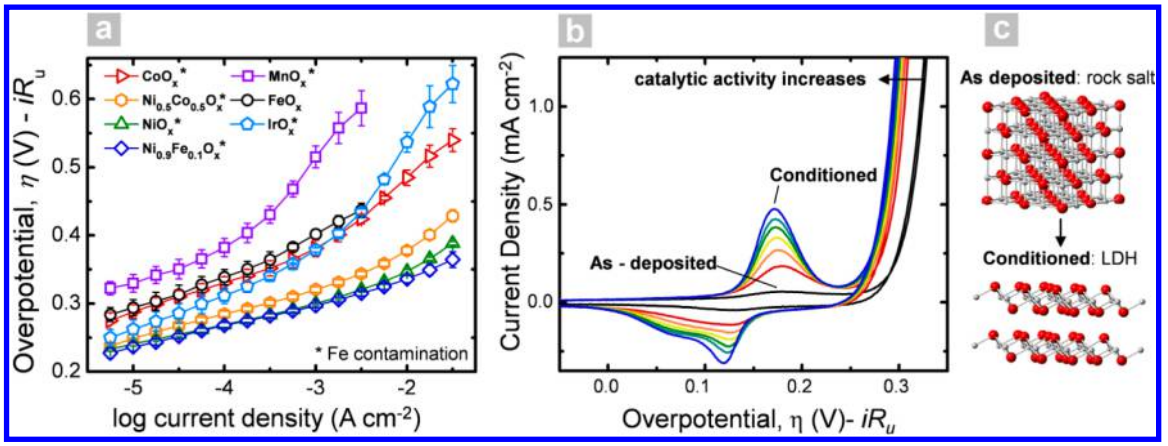

Figure 1. (a) Steady-state Tafel analysis of ultrathin films (i.e., 2−3 nm) of (nominally) oxides on Au/Ti substrates, (b) cyclic voltammetry of the electrochemical conditioning of NiO_x where each cycle shown was taken after 1 h anodization at 10 mA cm^{-2}, and (c) proposed in situ transformation of NiO_x during electrochemical conditioning (red = oxygen; white = $Ni^{2+/3+}$). All films were characterized in O_2 saturated 1 M KOH. Note that the data here is contaminated by electrolyte Fe impurities (marked with asterisk), which has a dramatic effect on the OER activity for the Ni-based samples in particular. Adapted from ref 34 with permission. Copyright 2012 American Chemical Society.

explaining simple activity trends. The Sabatier principle has become the generally accepted theory for understanding heterogeneous OER catalysis.[16] Surface metal cations (M) are believed to be the active sites for the OER. The reaction then proceeds through a series of intermediates (e.g., M−OH, M−O, M−OOH, M−OO), all bound by an M−O bond.[17] This mechanism suggests a relationship between activity and M−O bond strength that can be plotted to resemble a "volcano". Catalysts with optimal M−O bond strength are active and lie at the top of the "volcano", while those with too strong or too weak M−O bonds are worse catalysts with activities sloping down from the peak.[17,18]

While there have been numerous efforts to quantify activities experimentally, as well as efforts to predict them using computational methods, the intrinsic activity trends, particularly for earth-abundant first-row transition metals in alkaline conditions, are still not clear. For example, initial work by Delahay[19] showed that the OER overpotential trend at 1 A cm^{-2}, Co ≈ Fe > Cu > Ni, found by Hickling[20] could be correlated to M−OH bond strength. Trasatti later compiled data to determine that the empirical activity trend, RuO_2 > IrO_2 > MnO_2 > NiO > Co_3O_4 ≫ Fe_3O_4, correlated with the enthalpy of the reaction $MO_x + {}^1/_2O_2 \rightarrow MO_{x+1}$ (which should relate to the strength of the M−O bond).[21,22] An experimental activity trend of Ni > Co > Fe was found for electrochemically conditioned metallic electrodes in alkaline media studied by Lyons.[23] Near-monolayer metal (oxy)hydroxide films on Pt were characterized by Subbaraman,[24] leading to an activity trend of NiO_xH_y > CoO_xH_y > FeO_xH_y > MnO_xH_y. Computational analyses using density functional theory (DFT) have also yielded a range of trends. Calle-Vallejo[25] calculated an activity trend of NiO ≫ CoO ≈ FeO ≫ MnO, while Man[26] calculated Co_3O_4 > NiO > Mn_xO_y ≈ NiOb (where NiOb is a different surface construction). A number of trends have also been reported for perovskite oxide OER catalysts, for example, relating activity to the number of electrons in the e_g orbital of the metal cation.[27−29] These trends are complicated by many factors, including differences in electrochemically active surface area, catalyst electrical conductivity, surface chemical stability, and surface composition. The presence of electrolyte impurities such as Fe, which have been shown to substantially enhance the activity of both Ni- and Co-based catalysts (discussed in detail below),[30−33] is also critical to account for.

In this Perspective, we describe our efforts to uncover the intrinsic OER catalyst activity trends, to understand local structures and compositions responsible for catalysis, and to apply that knowledge in practically relevant systems. We discuss the role of secondary phenomena (such as electrical conductivity, mass transport, and chemical stability/solubility) on the measured activities and how these depend on structure, composition, and morphology. On the basis of these findings we provide a working model for mixed-metal Ni−Fe and Co−Fe (oxy)hydroxide OER catalysts, which we have shown exhibit the highest known activity in alkaline media.[34] This Perspective thus aims to provide insight into strategies to design catalysts that are intrinsically highly active and for their integration in industrially relevant alkaline electrolysis systems and emerging solar fuels devices.

2.0. THIN FILMS AS MODEL SYSTEMS

The study of OER catalysts has been complicated by many underlying confounding factors. For example, much work has been performed on poorly defined porous architectures which make comparisons of different materials difficult as the measured catalytic response is influenced by the active surface area and the electron/mass transport properties in a manner that is difficult to correct for.[35,36] Single crystals are in principle ideal systems, except they are difficult to grow with a range of compositions, often suffer from low electrical conductivity, and have surface structures that can rearrange during catalysis.

Our initial work focused on circumventing these issues using thin-film electrodes. With solution processing, we synthesized electrocatalyst films on quartz-crystal microbalance (QCM) electrodes so that the mass (and quantity of active material) could be measured and monitored in situ during electrocatalysis.[34] The films are spun-cast from ethanol solutions of metal salts mixed with surfactant to reduce surface tension and promote film formation. Quick (∼2 min), low-temperature (∼300 °C) annealing decomposes the nitrate anions and surfactant leaving an ∼2−3 nm thick layer of the desired oxide on the conductive electrode surface. In principle, the thin-film approach minimizes confounding effects due to mass and electron transport through typical thick, high-surface-area films

DOI: 10.1021/acs.chemmater.5b03148
Chem. Mater. 2015, 27, 7549−7558

or powders. It also reduces variations in real versus geometric surface area (i.e., roughness factors) because there is little material to support porosity. Using an electrochemical microbalance allowed for the calculation of lower-limit turnover frequencies (TOFs, defined as the number of O_2 molecules evolved per second per metal site) based on the mass of the catalyst films. The TOF is a lower limit because, even as a thin-film, all of the metal cations in the film may not be electrochemically accessible, and further, only a subset of the electrochemically accessible metal cation sites may be responsible for catalyzing the reaction (i.e., some sites may be more active than others, see further discussion in Section 3.0). We typically call this a lower-limit "total metal" turnover frequency, TOF_{tm}. The use of TOF_{tm} and the thin-film QCM approach has proved extremely valuable for establishing a common measurement basis and shows good agreement with other well-defined activity measurements.[7,37]

The thin-film measurements resulted in several surprising results (Figure 1a). First, precious-metal-based IrO_x, which is often found at the top of "volcano" activity plots for OER,[36] was not the most active material on a TOF_{tm} basis. IrO_x in fact had activities of the same order of magnitude as FeO_x and CoO_x and about 10-fold lower activity than the films prepared with Ni. Furthermore, in contrast to many previous reports that showed synergy between Co and Ni oxides for OER catalysis, $Ni_yCo_{1-y}O_x$ thin films showed decreasing activity relative to the pure NiO_x with increasing Co content. These results led us to study the Ni-based films in more detail to identify the underlying reason for the very high apparent activity.

We found from both the voltammetry (Figure 1b) and ex situ X-ray photoelectron spectroscopy (XPS) measurements that electrochemical conditioning caused a transformation from nanocrystalline NiO_x films to a layered (oxy)hydroxide that correlated to the increased activity (Figure 1a). This is consistent with equilibrium potential−pH diagrams (e.g., Pourbaix diagrams) that often show $Ni(OH)_2$ and NiOOH as the predominant species in neutral-to-basic aqueous solutions, at resting and OER potentials, respectively. In this Perspective we typically refer to these materials as (oxy)hydroxides and at times represent them with the general formula of MO_xH_y so as not to imply a specific oxidation or protonation state as these depend on both potential and pH.

Ni (oxy)hydroxide is used in commercial Ni-metal-hydride batteries and has been extensively studied. Dennis Corrigan, then at General Motors, discovered in the 1980s that Fe impurities had a dramatic effect on the self-discharge rate of $Ni(OH)_2$/NiOOH battery electrodes due to enhancement of OER catalytic activity.[32] We measured the Fe content in our thin film "NiO_x" electrodes after polarizing at OER potentials for 6 h and found that Fe now accounted for 10−20% of the transition-metal cations. The activity was further improved by adding 10% Fe to the initial precursor solution. The TOF_{tm} measured for $Ni(Fe)O_xH_y$ was >10-fold higher than for IrO_x control films and almost 2 orders of magnitude higher than that for CoO_x. $Ni(Fe)O_xH_y$ appeared to be the most-active material for OER in basic conditions known. This catalyst is almost certainly present on the surface of the stainless steel/Ni anodes used in commercial alkaline electrolyzers.

The very high intrinsic activity of $Ni(Fe)O_xH_y$ is fascinating and has stimulated a tremendous quantity of recent work focusing on different techniques to prepare $Ni(Fe)O_xH_y$ and related catalysts.[37−46] Many fundamental questions, however, remain. What is the role of Fe in the catalysis? Does Fe activate a Ni site or is Fe itself the "active site"? Does Fe incorporation affect other oxides/(oxy)hydroxides? Do other cation "impurities" increase activity via a similar mechanism? Can the composition and local structure be tuned to enhance activity further? What are the roles of mass and electron transport[47] inside the disordered (oxy)hydroxide structure in determining the apparent current response? Can these parameters be tuned for applications?

3.0. (OXY)HYDROXIDES AND HYDRATED OXIDES AS OER CATALYSTS

Our observation that nanocrystalline NiO was unstable with respect to the $Ni(OH)_2$/NiOOH phases during OER led us believe that perhaps many other conventionally studied oxide OER catalysts were unstable—at least in the near-surface region—relative to hydrated oxide or (oxy)hydroxide phases. Such electrolyte-permeated phases would have very different local structures and compositions than the parent oxides with the protonation state, coordination geometry, and oxidation state depending on the electrochemical potential and the electrolyte. Shao-Horn and co-workers, for example, found similar transformations in perovskite oxides,[48,49] though in some cases the bulk appeared to be stable.[50] Recent thermodynamic arguments show that indeed *no oxide* is theoretically stable under OER conditions because the driving force for lattice oxygen evolution exceeds that of oxygen evolution from the electrolyte.[51] Doyle has discussed extensively the role of hydrated surface layers in electrocatalysis.[52] The Co-oxide-phosphate[53] and Ni-oxide-borate[54] catalysts studied by Nocera and others are similarly hydrated electrolyte-permeated (oxy)hydroxide phases, and the "self-repair" mechanisms found appear to be related to this instability.[55]

Understanding the (oxy)hydroxide and hydrous surface phases therefore appears to be critical in understanding the OER, particularly in alkaline conditions. To study them, we synthesize electrolyte-permeated (oxy)hydroxides directly as thin films (with loading of ∼10 $\mu g\ cm^{-2}$) via electrodeposition at room temperature. Typically electrodeposition is from metal nitrates or from chloride salts with added sodium nitrate. The nitrate reduction reaction consumes protons near the electrode surface driving the direct precipitation of the hydroxide phase. This is a common deposition technique.[32,56,57] Anodic depositions can also be used, which rely on the solubility change upon metal cation oxidation to drive precipitation, typically of an oxyhydroxide, on the electrode surface. The resulting hydrated oxide or (oxy)hydroxide phases are, we hypothesize, similar or perhaps identical to those that would otherwise form in situ at the surface of oxide-based catalysts synthesized at high temperature.

The (oxy)hydroxide phases of NiO_xH_y and CoO_xH_y are particularly interesting. Their structure is composed of stacks of single atomic sheets of octahedrally coordinated metal cations (Figure 1c) typically yielding the nanoplatelet or leaflet film morphologies evident in Figure 2. Because the sheets are held together only by noncovalent bonds, the structures are often disordered, allowing for electrolyte access within the catalyst bulk and intersheet "galleries". In the case of NiO_xH_y every Ni can be electrochemically active (which is one reason it is used as a battery electrode).[34]

Role of Electrical Conductivity. The electrocatalytic activity of a metal cation site requires that the site is "electrically wired" to the metallic conductive current collector,

DOI: 10.1021/acs.chemmater.5b03148
Chem. Mater. 2015, 27, 7549−7558

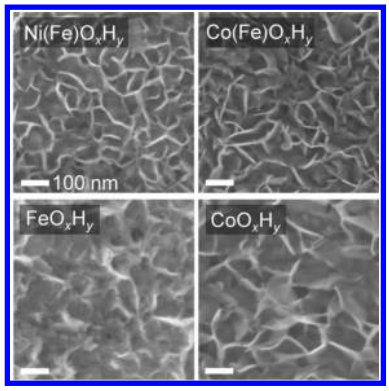

Figure 2. Scanning electron microscope images of the (oxy)hydroxide catalyst films. Images for CoO_xH_y and FeO_xH_y adapted from refs 33 and 58 with permission. Copyright 2015 American Chemical Society.

as well as "ionically wired" to the electrolyte solution. However, dry measurements of electronic conductivity, for example, on pressed oxide powders,[28] are not relevant to the hydrated surface phases where catalysis takes place. To make in situ conductivity measurements, we used microfabricated interdigitated array (IDA) electrodes (Figure 3).[30,33] The catalyst is

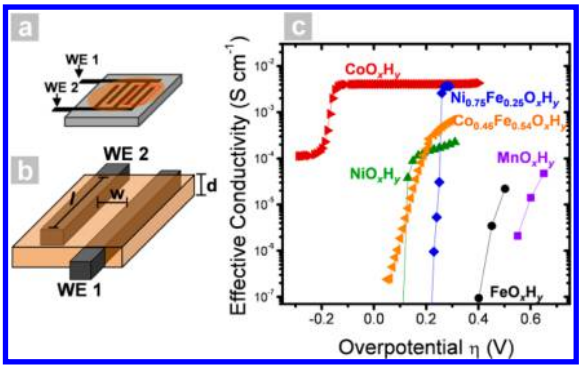

Figure 3. In situ electrical conductivity measurements. (a) Interdigitated array electrode (IDA) and (b) expanded portion the IDA where w is the gap spacing (2 μm), d is the film thickness, and l is the electrode length (2 mm). (c) Effective conductivity measured in 1 M KOH with a 10 mV DC offset between the two working electrodes. Adapted froms ref 33 and 58 with permission. Copyright 2015 American Chemical Society.

electrodeposited so that it bridges the gap between the "fingers" of the IDA. The conductivity measurement is made using a bipotentiostat (or a single-channel potentiostat in conjunction with a source-meter unit). A small DC bias (typically 10 mV) is applied across the two sets of fingers (WE1 and WE2 in Figure 3) while the potential of both WE1 and WE2 is controlled relative to the reference electrode in the electrochemical cell. The magnitude of the DC current measured at steady-state can be related to the electrical conductivity of the film at a given state of charge. Some care must be taken in the measurement when the electrical conductivity is very low (e.g., for FeO_xH_y), because background faradaic currents can complicate measurement of the underlying DC conductivity current (see particularly the Supporting Information in ref 33).

The effective conductivity measurements of the first-row transition metal (oxy)hydroxides were found to vary dramatically with composition and with electrochemical potential (Figure 3c). For the Ni- and Co-based (oxy)hydroxides we found that the catalysts were electrically insulating in the 2^+ resting oxidation state but were quite conductive after oxidation under OER conditions to the (nominally) 3^+ state. Interestingly, Fe doping increased the conductivity of NiOOH but decreased that of CoOOH. However, all the Ni- and Co-based catalysts were sufficiently conductive (with or without the added Fe) such that the potential drop due to catalyst resistivity would be negligible (<0.1 mV) for the typical films studied (that are, at most, a few hundred nanometers thick). FeO_xH_y and MnO_xH_y, however, exhibited high resistivity until much higher overpotentials. We noticed that the onset of electrical conductivity correlated with the onset of OER activity, suggesting that, for the Fe and Mn (oxy)hydroxides, the poor electrical conductivity was "gating" the electrocatalysis.

Quantifying Electrolyte Accessibility and "Counting" Electrochemically Active Sites. As mentioned above, the layered double hydroxide structure adopted by many of the relevant first-row transition-metal OER catalysts has weak noncovalent interactions between the metal cation sheets that allows for disordered structures with high electrolyte accessibility. Quantifying the precise number of accessible cations is important, however, to estimate TOFs, especially in systems which may have different structure types.

For an "ideal" dense oxide catalyst, i.e., with no surface hydrated phase, only the surface atoms are electrochemically accessible. The number could be calculated from the surface area obtained, for example, from gas adsorption measurements. If the oxide catalyst is sufficiently conductive, the electrode capacitance, derived from electrochemical impedance measurements can also be used to estimate surface area based on known areal capacitances.[59,60] We caution, however, that impedance measurements generally fail for estimating the surface areas of hydrated catalysts. The capacitance of the underlying conductive electrode is often measured, as the electrolyte permeates through the catalyst layer.[37,61]

For the Ni and Co (oxy)hydroxide catalysts, the number of electrochemically accessible metal cations can be calculated by integrating the pre-OER redox features evident in the voltammetry (Figure 4). Care must be taken, however, to ensure that the oxidation wave is collected under conditions where the film is in a completely reduced state (i.e., Co^{2+} or Ni^{2+}). It has been documented for the Ni[61−63] and Co[33] (oxy)hydroxides that, due to the conductivity switching behavior illustrated in Figure 3, the integrated charge in the waves collected from repeated cycling only count a fraction of the electrochemically accessible metal centers when films are thicker than a few nanometers. Holding at a reducing potential for ~20 min or letting the sample sit at open circuit for a long period allows the oxidized catalyst that is isolated from the conducting substrate by the reduced metal hydroxide to discharge.[61] Integrating the first oxidation wave then yields the total number of electrochemically accessible sites.

For Ni (oxy)hydroxide, up to 1.6 e^- per Ni have been reported during oxidation. We simultaneously measure mass by QCM. If we assume the film is composed of $Ni_xFe_{1-x}(OH)_2$ and ignore additional solvent or electrolyte weight, then we find almost exactly 1 e^- per Ni. These results lead us to the conclusion that nearly all the Ni cations in the $Ni(Fe)O_xH_y$ films are electrochemically accessible. For CoO_xH_y, only about 60% of the Co ions are electrochemically active, while for $Co_{0.5}Fe_{0.5}O_xH_y$ they are nearly all electrochemically active (assuming 1 e^- per Co). This type of catalyst has been termed to exhibit "volume" activity.[64] Because the integrated redox

DOI: 10.1021/acs.chemmater.5b03148
Chem. Mater. 2015, 27, 7549−7558

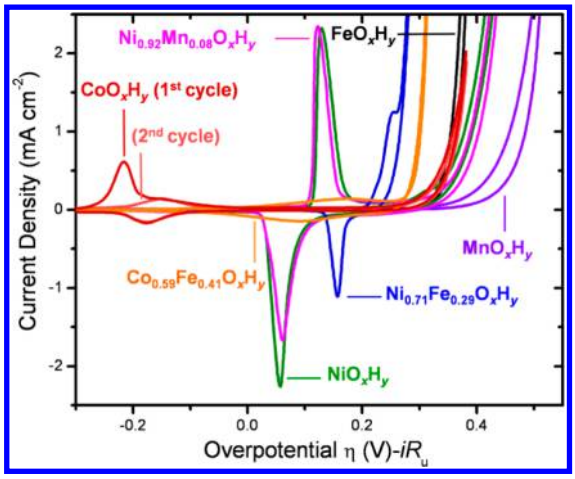

Figure 4. Voltammetry of electrodeposited hydrated OER catalysts in 1 M KOH collected at 10 mV s^{-1}, each at a loading between ~7 and 12 μg cm^{-2}. The prewave redox features for the Ni and Co can be used to calculate the fraction of active sites as long as care is taken to ensure that the integrated charge in the wave is not limited by conductivity switching.[61] Both the first and the second cycles of CoO_xH_y are shown. Integration of the oxidation wave for the first cycle, i.e., starting with the film completely reduced, provides for an accurate measurement of the total electrolyte-accessible Co or Ni ions. Adapted from ref 58 with permission. Copyright 2015 American Chemical Society.

wave measurements show that most of the cation sites are electrochemically accessible, we typically calculated lower-limit TOFs based on the total number of all cations obtained from the "total-metal" mass of the film measured using the QCM electrode (TOF_{tm}). We ignore the mass contributions from electrolyte solvent or ions, because these corrections are small relative to the orders-of-magnitude variation in TOF_{tm}.

Estimating the number of electrochemically accessible cations is not possible for FeO_xH_y and MnO_xH_y using redox peak integration because they have low conductivity and do not show substantial reversible faradaic chemistry. The very low conductivity also indicates that only those cations within the electrolyte-permeated solid very close to the conductive support (typically Au or Pt in our case) are able to contribute to the OER. TOF_{tm} calculated from the total mass of thick films thus severely underestimates the intrinsic per-Fe activity. For FeO_xH_y on Au, however, TOFs obtained for very thin films appear to be enhanced by substrate interactions.[58]

"Intrinsic" Activity Trends for Oxyhydroxides in the Presence and Absence of Fe Impurities. Understanding the intrinsic catalytic activity provides insight into improved catalyst design. As described in the introduction, however, experimental and computationally predicted activity trends have varied substantially. The "real" trends, particularly for the first-row transition metals, are likely to have been obscured by electrolyte impurities, potential-dependent electrical conductivity, and difficulty in correcting for surface-area or mass-loading differences. One of our central goals is to provide revised activity trends in the absence of these confounding effects. These should provide a new basis for comparison to theory and help guide the design of improved catalyst systems.

We used the interdigitated electrodes to measure the electrical conductivity in situ of each catalyst and determine whether or not the measured activities are affected by poor electronic transport. We used the thin-film QCM approach to measure the mass of the films in situ and ensure that they are not dissolving on the time scale of the activity measurement. We also developed simple methods to rigorously clean the electrolyte of Fe.[30,33] Because both $Co(OH)_2$ and $Ni(OH)_2$ have a high affinity for free Fe^{3+} in KOH, we use precipitated Ni or Co hydroxides as powders to absorb the Fe from the electrolyte. We then centrifuge and decant the purified electrolyte directly into an acid-cleaned and glass-free electrochemical cell where we test CoO_xH_y or NiO_xH_y as thin films. When we do this we observe no Fe by XPS analysis in the catalyst films. The catalyst material itself, in powder form, thus serves to purify the electrolyte used to test the catalyst thin films. To understand possible substrate enhancement effects, we measure activities on both Au and Pt QCM crystals.

Our results (Figure 5a,b) establish a new activity trend for OER catalysts.[58] We have plotted the activity trend at both η =

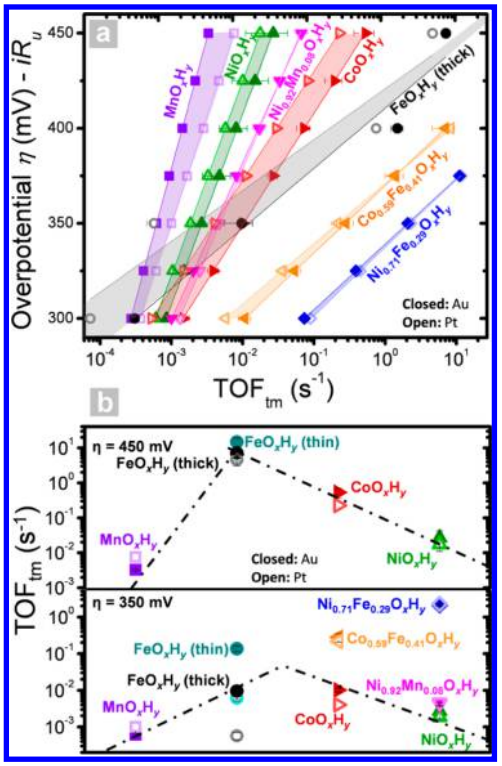

Figure 5. (a) Steady-state activity trends as a function of potential for (oxy)hydroxides on Au (solid) and Pt (open) quartz crystals. (b) at η = 450 mV (top) and at η = 350 mV (bottom). Compositions in (b) are ordered based on atomic number of the host/primary cation. TOF_{tm} is calculated from total number of metal cations based on in situ mass measurements. Lines and shading lines are to guide the eye. All the films had a loading of between 8 and 12 μg cm^{-2}, except for the thin FeO_xH_y which was 0.5−1.0 μg cm^{-2}. Adapted from ref 58 with permission. Copyright 2015 American Chemical Society.

350 mV and at η = 450 mV. The lower η is most relevant for applications, but there is substantial uncertainty in calculating the apparent activity of FeO_xH_y because it depends strongly on the film thickness and substrate identity (since only the cations near the substrate surface are active).[58] At η = 450 mV, FeO_xH_y is more conductive and thus the apparent activity is largely insensitive to support interactions and film thickness—more of the electrolyte-permeated FeO_xH_y film contributes to the OER activity. These activity trends for the first-row transition metals are substantially different than those previously reported. While Ni-based oxides and (oxy)hydroxides are often thought to be

DOI: 10.1021/acs.chemmater.5b03148
Chem. Mater. 2015, 27, 7549−7558

the most-active first-row OER catalysts, this is due to Fe impurities. NiO_xH_y without Fe impurities is at least three-orders-of-magnitude less active for OER than $Ni(Fe)O_xH_y$. We found similar behavior for NiO_xH_y and $Ni(Fe)O_xH_y$ in near-neutral borate buffer solutions,[31] as well as for CoO_xH_y and $Co(Fe)O_xH_y$.[33] While many studies have found Fe oxide/(oxy)hydroxide catalysts to be inactive,[24,36] this appears to be primarily due to their very low electrical conductivity.

4.0. ROLE OF Fe IN ACTIVATING OER CATALYSTS

The very high intrinsic OER activity of $Ni(Fe)O_xH_y$ and $Co(Fe)O_xH_y$ motivated our efforts to understand the fundamental roles of Fe and the layered double (oxy)hydroxide structure in OER catalysis. We have proposed a new model for the OER on mixed-metal (oxy)hydroxides (Figure 6).[33,58] Our

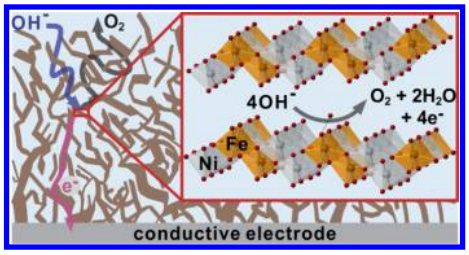

Figure 6. Schematic of active electrolyte-permeated catalyst structure. OER likely occurs at the Fe sites (orange) while the NiOOH host (gray) supports electronic transport and chemically stabilizes the Fe. Mass transport of OH^- and O_2 is facilitated by the open disordered structure and weak noncovalent interactions between the (oxy)-hydroxide layers.

hypothesis is that Fe—whether introduced intentionally or from electrolyte impurities—is the active site in *essentially all* of the highly active first-row transition metal oxide OER catalysts previously reported. When Ni or Co is present, (oxy)hydroxide phases form that accommodate the Fe by substituting for Co or Ni, which we find evidence for from X-ray diffraction experiments on $Ni(Fe)O_xH_y$ and $Co(Fe)O_xH_y$.[30,33]

The Ni or Co (oxy)hydroxide host provides several functions. When oxidized it is conductive and thus electrically connects the dispersed Fe sites to the conducting electrode. It also serves as an intrinsically high-surface-area support with nearly every metal cation electrochemically accessible. The electronic interaction between Ni/Co and Fe, evident from the dependence of the Ni/Co redox potential on the Fe content,[56,65] likely further activates the Fe site for OER, while also chemically stabilizing Fe from dissolution (as demonstrated by the data in Figure 7).

Several other lines of evidence also support our proposed model. First, pure FeO_xH_y is much more active than previously thought, and the apparent activity is limited by poor electrical conductivity. In other words, only the first monolayer or so of FeO_xH_y supported on a metallic electrode is active for OER.[66] The *iR* voltage drop to access Fe further from the substrate dramatically reduces the driving force available for OER. This interpretation is consistent with our finding that the Tafel slope and geometric activity of FeO_xH_y films remain constant even though a dramatic mass loss from the film is measured (Figure 7, bottom panel). Because only Fe directly in contact with the Au substrate is active for OER, dissolution of the remainder of the film does not affect the measured current. Fundamental

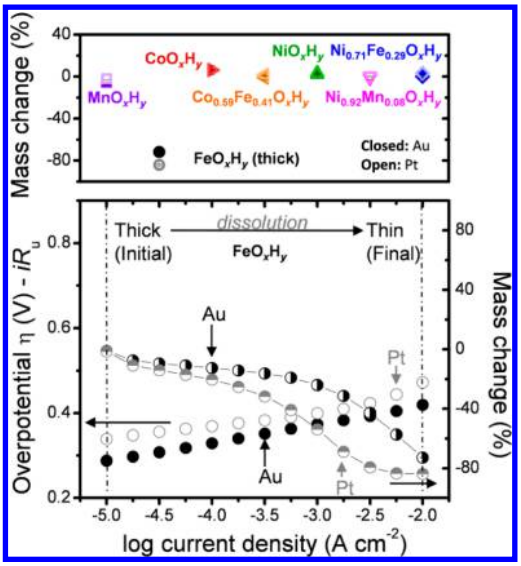

Figure 7. Top panel shows the mass change for a variety of first-row transition metals during an ~50 min steady-state Tafel analysis (closed symbols, Au and open symbols, Pt), and the bottom panel shows the steady-state Tafel analysis (left axis) of FeO_xH_y with in situ mass (right axis) on Au and Pt substrates. Adapted from ref 58. Copyright 2015 American Chemical Society.

aspects of the OER on FeO_xH_y and support interactions deserve further study.

The observation that Fe doping enhances the OER activity of Ni (oxy)hydroxide[30−32,34,41,42,65,67,68] and Co (oxy)-hydroxide,[33] by factors of roughly three and two orders of magnitude, respectively, is also consistent with the proposed model.[33,69−71] Tafel slopes for $Ni(Fe)O_xH_y$ and $Co(Fe)O_xH_y$ are both near 30 mV dec^{-1} and within the range measured for pure FeO_xH_y (~30−45 mV dec^{-1}), suggesting a similar mechanism in all Fe-containing catalysts. We also showed that the activity of $Co_{1-z}(Fe)_zO_xH_y$ can be modeled as a function of z assuming a constant intrinsic TOF at η = 350 mV for both Fe (0.8 s^{-1}) and Co (0.006 s^{-1}) sites (TOF_{Fe}^{app} and TOF_{Co}^{app}, respectively). These TOF estimates are based on experimental activity measurements.[33] Similar analysis can be applied to $Ni(Fe)O_xH_y$.[67] We acknowledge, however, that these analyses cannot distinguish between Fe acting as the active site or an adjacent, activated Ni/Co doing so. However, the observation of high TOF in thin, pure FeO_xH_y is most consistent with the hypothesis that Fe is the active site.

Friebel et al. provide further evidence for Fe as the OER active site.[68] Operando X-ray absorption (XAS) measurements of $Ni_{1-x}Fe_xOOH$ showed that Fe^{3+} occupies octahedral Ni sites in the (oxy)hydroxide structure (for x < 0.25) with unusually short Fe−O bond distance ~6% less than that in γ-FeOOH. Using DFT computational methods, this structural motif was found to have more-optimal adsorption energies for OER intermediates, and thus lower theoretical overpotentials, relative to Ni sites in $Ni_{1-x}Fe_xOOH$. While there remain questions regarding the degree to which the simplified physical systems accessible to current DFT calculations represent the reality of the electrochemical system, these results support strongly the hypothesis that Fe is the active site in $Ni(Fe)O_xH_y$.

It is also interesting that, for Fe contents above roughly 25−50%, Friebel finds evidence for phase-segregated FeOOH and lowered overall geometric activity. This is consistent with our results showing FeOOH is electrically insulating and thus OER

DOI: 10.1021/acs.chemmater.5b03148
Chem. Mater. 2015, 27, 7549−7558

inactive. It is also consistent with our observation of substantial mass loss during OER from $Co_{1-x}Fe_xOOH$ for $x > 60\%$ which is thus presumably due to chemical dissolution of phase-segregated FeOOH. Targeting multication matrices with high Fe content that preserve electrical conductivity at low overpotentials and chemically stabilize Fe is thus a possible strategy for further improving OER performance in these systems.

5.0. DESIGN OF OPTIMIZED Ni–Fe OXYHYDROXIDE OER CATALYSTS

While the thin-film experiments described above provide a fundamental understanding of the OER on oxides and (oxy)hydroxides, practical systems, e.g., for alkaline electrolysis, require much higher mass loadings. Because all the metal cations are electrochemically accessible for Ni–Fe (oxy)-hydroxide, the catalytic current at a given overpotential should increase linearly with loading—*if* the electrical resistance of the catalyst film and the mass-transport and ionic resistances within the electrolyte-permeated catalyst remain negligible. A number of advanced architectures have been studied to improve Ni–Fe oxyhydroxide activity at high mass loading. For example, hybrid structures using carbon nanotubes[41] or graphene[43] have been fabricated to improve electrical conductivity. Graphitic carbon, while stable for lab time scales in test-cells, is unlikely to be stable long-term in an alkaline electrolyzer (~80 °C in concentrated base). Approaches to increase active-site accessibility and reduce mass-transfer effects at high loading include Al dissolution from Ni–Al to from porous Ni electrodes,[72,73] deposition onto, followed by dissolution of, polystyrene sphere templates,[74] and deposition of active Ni–Fe (oxy)hydroxide layers onto porous metallic Ni foams.[39,40,44]

We have focused on controlling the electrodeposition process to access thick morphologies of Ni–Fe (oxy)hydroxide that retain the high intrinsic TOF of the thin-film samples used for fundamental studies. Typically we use a continuous cathodic electrodeposition at a constant current to drive nitrate reduction and cause precipitation of the hydroxides on the electrode. This leads to an open, "fluffy" catalyst architecture, as shown in Figure 8c. As we increase loading the geometric activity does increase, but the intrinsic per-metal TOF decreases by almost a factor of 5. Interestingly we notice that the charge reversibility, i.e., the ratio of the charge in the Ni oxidation wave measured on the first cycle relative to that measured at steady state,[61] decreases similarly to TOF. As discussed above, a reversibility below unity is attributed to the conductivity switching of the Ni (oxy)hydroxide and trapping of a portion of the film in the oxidized state upon reduction.[33,61–63] Therefore, films that are better electrically connected with the conducting support should have higher reversibility.

We developed a simple pulsed-electrodeposition process, where, following each 2 s deposition current pulse at −10 mA cm^{-2}, the solution is stirred for ~10 s to reinfiltrate the deposited (porous) catalyst with fresh solution precursor. Pulsed deposition eliminates the decrease in the TOF_{tm} with increased mass loading resulting from continuous deposition (Figure 8a), which we attribute to improved electrical connectivity (and likely smaller domain size) in the Ni–Fe (oxy)hydroxide sheets. This hypothesis is supported by the correlation between enhanced TOF and electrochemical reversibility at high loadings observed for the pulsed-deposited films. These films perform comparably to those with more-

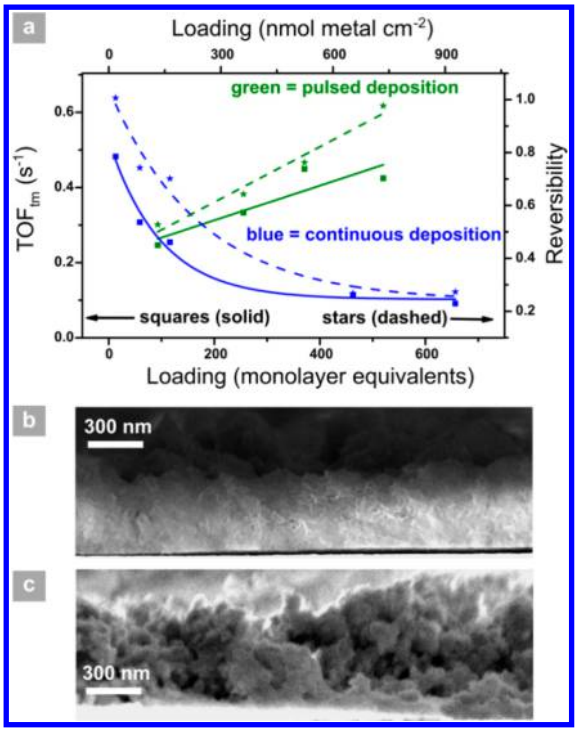

Figure 8. (a) Loading-dependent reversibility (stars, dashed lines) and activity (squares, solid lines) of pulse (green) and continuously (blue) deposited films. The lines are drawn to illustrate trends. The reversibility is the ratio of metal centers measured during the first cathodic return sweep and the first anodic forward sweep during voltammetry. The data shown was collected on Au electrodes at 10 mV s^{-1}. TOF activity data were obtained from chronoamperometry (*iR* corrected) and normalized with loadings determined using integration of the anodic wave in the first cycle. Cross-sectional SEM images of the (b) pulse and (c) continuously deposited films deposited under conditions resulting in the highest loading films shown in (a). Figure adapted from ref 61 with permission. Copyright 2015 American Chemical Society.

advanced architectures,[39,41,43] for example, passing a current density of 120 mA cm^{-2} at 300 mV overpotential in 1 M KOH at room temperature with a loading of 730 nmol metal cm^{-2}. Given the temperature activation of the OER on Ni–Fe oxyhydroxides (E_a ~ 25–30 kJ mol^{-1}),[75] roughly five times higher activity would be expected at typical operating conditions of 80 °C. By using Ni foam instead of planar metallic supports, the geometric activity could also be significantly increased.

6.0. CONCLUSION AND OUTLOOK

The work described here supports a new view of OER catalysis. Thermodynamics appear to favor hydrated phases, like (oxy)hydroxides or hydrous oxides, over crystalline oxides under OER conditions. Fe impurities, which are ubiquitous in neutral to alkaline electrolytes, dramatically enhance the activities of Ni and Co-based OER catalysts. The most-active structures are those where Fe is supported within a Ni or Co (oxy)hydroxide host. The active site is probably Fe, while the host provides an electrically conductive and high-surface-area framework that chemically stabilizes and further activates the Fe sites. These Fe-activated Ni and Co OER catalyst architectures are ubiquitous. They are likely the active structures in essentially all of the vast number of reports on OER catalysis with Ni or Co and Fe (intentionally or unintentionally

DOI: 10.1021/acs.chemmater.5b03148
Chem. Mater. 2015, 27, 7549–7558

introduced) in neutral to basic conditions, independent of preparation method.[8,27,28,37,38,52,55,76−82]

Despite advances in understanding what the OER active phases and compositions are, the details of the mechanism are still difficult to unambiguously determine.[68,83] Given rapid improvements in in situ measurements at synchrotron X-ray sources, there appears significant opportunity to study hydrated OER catalysts in their active state and understand how the electronics[84−86] and structure[48,68,87−89] of the catalysts evolve during the OER. The insight gained from composition-activity-structure analysis should help in the formulation of improved computational methods that better model the active-state structure, including the surrounding solvent and ionic environment as a function of the applied potential.[90]

Finally, in order for the fundamental work to impact applications, the catalysts must be studied under practical test conditions. Often, catalysts that show high activities in analytical three-electrode cells do not perform well in commercially relevant devices that demand high current densities and operating temperatures with long lifetimes. Traditional alkaline electrolyzers probably can be improved by tuning the OER catalyst architecture and composition,[11,91] but dramatic improvements over conventional stainless steel/Ni electrodes will be challenging. Alkaline membrane electrolyzers that utilize a hydroxide-conducting membrane[14] and earth-abundant catalysts might be able to reach the high performance of current proton-exchange (acid) membrane electrolyzers that require Pt and IrO_2 catalysts. To do this, however, advances in hydroxide membrane stability are needed,[92,93] as well as further research on approaches to enable catalyst/ionomer composites that provide good electronic and ionic conductivities.

AUTHOR INFORMATION

Corresponding Author

*E-mail: swb@uoregon.edu.

Author Contributions

All authors contributed to the preparation of this manuscript.

Notes

The authors declare no competing financial interest.

Biography

Shannon Boettcher is an associate professor at the University of Oregon in the Department of Chemistry and Biochemistry. He received his B.A. in chemistry with a physics minor at the University of Oregon in 2003 where he was a Barry M. Goldwater Scholar. He received his Ph.D. in Inorganic Materials Chemistry with Galen Stucky at UC Santa Barbara in 2008 where he was an NSF Graduate Research and UC Chancellor's Fellow. As a Kavli Nanoscience Institute Prize Postdoctoral Scholar, he studied three-dimensional Si structures for solar energy conversion and storage at the California Institute of Technology working with Nate Lewis (Chemistry) and Harry Atwater (Applied Physics). In 2010, he joined the Chemistry Department at the University of Oregon, and in 2011 was named one of 18 DuPont Young Professors worldwide. In 2014 he was named a Cottrell Scholar and in 2015 a Sloan Fellow and Camille Dreyfus Teacher-Scholar Awardee. His research focuses on the design and understanding of inorganic materials systems for energy conversion and storage.

ACKNOWLEDGMENTS

This work was supported by the National Science Foundation through CHE-1301461. S.Z. acknowledges the China Scholar Council for financial support. A.S.B acknowledges support from the United States Air Force in conjunction with the United States Air Force Academy faculty pipeline program. The authors thank Kathy Ayers and Julie Renner from Proton OnSite for insight into PEM and AEM electrolyzer engineering, and Lena Trotochaud, Adam Smith, and Matt Kast for their contributions to the original research. S.W.B. thanks the Research Corporation for Science Advancement, the Sloan Foundation, and the Camille and Henry Dreyfus Foundation for additional support.

REFERENCES

(1) Walter, M. G.; Warren, E. L.; McKone, J. R.; Boettcher, S. W.; Mi, Q.; Santori, E. a; Lewis, N. S. Solar Water Splitting Cells. *Chem. Rev.* **2010**, *110* (11), 6446−6473.

(2) Ursua, A.; Gandia, L. M.; Sanchis, P. Hydrogen Production From Water Electrolysis: Current Status and Future Trends. *Proc. IEEE* **2012**, *100* (2), 410−426.

(3) Mckone, J. R.; Lewis, N. S.; Gray, H. B. Will Solar-Driven Water-Splitting Devices See the Light of Day? *Chem. Mater.* **2014**, *26*, 407−414.

(4) Lewis, N. S.; Nocera, D. G. Powering the Planet: Chemical Challenges in Solar Energy Utilization. *Proc. Natl. Acad. Sci. U. S. A.* **2006**, *103* (43), 15729−15735.

(5) Turner, J. A. Sustainable Hydrogen Production. *Science* **2004**, *305* (5686), 972−974.

(6) Pinaud, B. A.; Benck, J. D.; Seitz, L. C.; Forman, A. J.; Chen, Z.; Deutsch, T. G.; James, B. D.; Baum, K. N.; Baum, G. N.; Ardo, S.; Wang, H.; Miller, E.; Jaramillo, T. F. Technical and Economic Feasibility of Centralized Facilities for Solar Hydrogen Production via Photocatalysis and Photoelectrochemistry. *Energy Environ. Sci.* **2013**, *6* (7), 1983−2002.

(7) Trotochaud, L.; Boettcher, S. W. Precise Oxygen Evolution Catalysts: Status and Opportunities. *Scr. Mater.* **2014**, *74*, 25−32.

(8) Galán-Mascarós, J. R. Water Oxidation at Electrodes Modified with Earth-Abundant Transition-Metal Catalysts. *ChemElectroChem* **2015**, *2* (1), 37−50.

(9) Zeng, K.; Zhang, D. Recent Progress in Alkaline Water Electrolysis for Hydrogen Production and Applications. *Prog. Energy Combust. Sci.* **2010**, *36* (3), 307−326.

(10) Carmo, M.; Fritz, D. L.; Mergel, J.; Stolten, D. A Comprehensive Review on PEM Water Electrolysis. *Int. J. Hydrogen Energy* **2013**, *38* (12), 4901−4934.

(11) Pletcher, D.; Li, X. Prospects for Alkaline Zero Gap Water Electrolysers for Hydrogen Production. *Int. J. Hydrogen Energy* **2011**, *36* (23), 15089−15104.

(12) Li, X.; Walsh, F. C.; Pletcher, D. Nickel Based Electrocatalysts for Oxygen Evolution in High Current Density, Alkaline Water Electrolysers. *Phys. Chem. Chem. Phys.* **2011**, *13* (3), 1162−1167.

(13) Ayers, K. E.; Anderson, E. B.; Capuano, C.; Carter, B.; Dalton, L.; Hanlon, G.; Manco, J.; Niedzwiecki, M. Research Advances towards Low Cost, High Efficiency PEM Electrolysis. *ECS Trans.* **2010**, *33* (1), 3−15.

(14) Leng, Y.; Chen, G.; Mendoza, A. J.; Tighe, T. B.; Hickner, M. A.; Wang, C.-Y. Solid-State Water Electrolysis with an Alkaline Membrane. *J. Am. Chem. Soc.* **2012**, *134* (22), 9054−9057.

(15) Marini, S.; Salvi, P.; Nelli, P.; Pesenti, R.; Villa, M.; Berrettoni, M.; Zangari, G.; Kiros, Y. Advanced Alkaline Water Electrolysis. *Electrochim. Acta* **2012**, *82*, 384−391.

(16) Sabatier, F. *La Catalyse En Chimie Organique*; Berauge: Paris, 1920.

(17) Rossmeisl, J.; Qu, Z.-W.; Zhu, H.; Kroes, G.-J.; Nørskov, J. K. Electrolysis of Water on Oxide Surfaces. *J. Electroanal. Chem.* **2007**, *607* (1−2), 83−89.

(18) Man, I. C.; Su, H. Y.; Calle-Vallejo, F.; Hansen, H. a.; Martínez, J. I.; Inoglu, N. G.; Kitchin, J.; Jaramillo, T. F.; Nørskov, J. K.; Rossmeisl, J. Universality in Oxygen Evolution Electrocatalysis on Oxide Surfaces. *ChemCatChem* **2011**, *3*, 1159−1165.

DOI: 10.1021/acs.chemmater.5b03148
Chem. Mater. 2015, 27, 7549−7558

(19) Ruetschi, P.; Delahay, P. Influence of Electrode Material on Oxygen Overvoltage - a Theoretical Analysis. *J. Chem. Phys.* **1955**, *23* (3), 556−560.
(20) Hickling, A.; Hill, S. Oxygen Overvoltage. Part I. The Influence of Electrode Material, Current Density, and Time in Aqueous Solution. *Discuss. Faraday Soc.* **1947**, *1*, 236−246.
(21) Trasatti, S. Electrocatalysis in the Anodic Evolution of Oxygen and Chlorine. *Electrochim. Acta* **1984**, *29* (11), 1503−1512.
(22) Trasatti, S. Electrocatalysis by Oxides - Attempt at a Unifying Approach. *J. Electroanal. Chem. Interfacial Electrochem.* **1980**, *111*, 125−131.
(23) Lyons, M. E. G.; Brandon, M. P. A Comparative Study of the Oxygen Evolution Reaction on Oxidised Nickel, Cobalt and Iron Electrodes in Base. *J. Electroanal. Chem.* **2010**, *641* (1−2), 119−130.
(24) Subbaraman, R.; Tripkovic, D.; Chang, K.-C.; Strmcnik, D.; Paulikas, A. P.; Hirunsit, P.; Chan, M.; Greeley, J.; Stamenkovic, V.; Markovic, N. M. Trends in Activity for the Water Electrolyser Reactions on 3d M(Ni,Co,Fe,Mn) Hydr(oxy)oxide Catalysts. *Nat. Mater.* **2012**, *11* (6), 550−557.
(25) Calle-Vallejo, F.; Díaz-Morales, O. A.; Kolb, M. J.; Koper, M. T. M. Why Is Bulk Thermochemistry a Good Descriptor for the Electrocatalytic Activity of Transition Metal Oxides? *ACS Catal.* **2015**, *5* (2), 869−873.
(26) Man, I. C.; Su, H. Y.; Calle-Vallejo, F.; Hansen, H. a.; Martínez, J. I.; Inoglu, N. G.; Kitchin, J.; Jaramillo, T. F.; Nørskov, J. K.; Rossmeisl, J. Universality in Oxygen Evolution Electrocatalysis on Oxide Surfaces. *ChemCatChem* **2011**, *3* (7), 1159−1165.
(27) Suntivich, J.; May, K. J.; Gasteiger, H. A.; Goodenough, J. B.; Shao-Horn, Y. A Perovskite Oxide Optimized for Oxygen Evolution Catalysis from Molecular Orbital Principles. *Science* **2011**, *334* (6061), 1383−1385.
(28) Bockris, J. O.; Otagawa, T. The Electrocatalysis of Oxygen Evolution on Perovskites. *J. Electrochem. Soc.* **1984**, *131* (2), 290−302.
(29) Bockris, J. O.; Otagawa, T. Mechanism of Oxygen Evolution on Perovskites. *J. Phys. Chem.* **1983**, *87* (15), 2960−2971.
(30) Trotochaud, L.; Young, S. L.; Ranney, J. K.; Boettcher, S. W. Nickel−Iron Oxyhydroxide Oxygen-Evolution Electrocatalysts: The Role of Intentional and Incidental Iron Incorporation. *J. Am. Chem. Soc.* **2014**, *136* (18), 6744−6753.
(31) Smith, A. M.; Trotochaud, L.; Burke, M. S.; Boettcher, S. W. Contributions to Activity Enhancement via Fe Incorporation in Ni-(oxy)hydroxide/borate Catalysts for near-Neutral pH Oxygen Evolution. *Chem. Commun.* **2015**, *51* (25), 5261−5263.
(32) Corrigan, D. A. The Catalysis of the Oxygen Evolution Reaction by Iron Impurities in Thin Film Nickel Oxide Electrodes. *J. Electrochem. Soc.* **1987**, *134* (2), 377.
(33) Burke, M. S.; Kast, M. G.; Trotochaud, L.; Smith, A. M.; Boettcher, S. W. Cobalt-Iron (oxy)hydroxide Oxygen Evolution Electrocatalysts: The Role of Structure and Composition on Activity, Stability, and Mechanism. *J. Am. Chem. Soc.* **2015**, *137*, 3638−3648.
(34) Trotochaud, L.; Ranney, J. K.; Williams, K. N.; Boettcher, S. W. Solution-Cast Metal Oxide Thin Film Electrocatalysts for Oxygen Evolution. *J. Am. Chem. Soc.* **2012**, *134* (41), 17253−17261.
(35) Matsumoto, Y.; Sato, E. Electrocatalytic Properties of Transition-Metal Oxides for Oxygen Evolution Reaction. *Mater. Chem. Phys.* **1986**, *14* (5), 397−426.
(36) Trasatti, S.; Lodi, G. Oxygen and Chlorine Evolution at Conductive Metallic Oxide Anodes. In *Electrodes of Conductive Metallic Oxides*; Trasatti, S., Ed.; Elsevier: Amsterdam, 1981; Vol. *B*, pp 521−626.
(37) Fominykh, K.; Chernev, P.; Zaharieva, I.; Sicklinger, J.; Stefanic, G.; Döblinger, M.; Müller, A.; Pokharel, A.; Böcklein, S.; Scheu, C.; Bein, T.; Fattakhova-Rohlfing, D. Iron-Doped Nickel Oxide Nanocrystals as Highly Efficient Electrocatalysts for Alkaline Water Splitting. *ACS Nano* **2015**, *9* (5), 5180−5188.
(38) Smith, R. D. L.; Prévot, M. S.; Fagan, R. D.; Zhang, Z.; Sedach, P. A.; Siu, M. K. J.; Trudel, S.; Berlinguette, C. P. Photochemical Route for Accessing Amorphous Metal Oxide Materials for Water Oxidation Catalysis. *Science* **2013**, *340* (6128), 60−63.
(39) Lu, X.; Zhao, C. Electrodeposition of Hierarchically Structured Three-Dimensional Nickel−Iron Electrodes for Efficient Oxygen Evolution at High Current Densities. *Nat. Commun.* **2015**, *6*, 6616.
(40) Lu, Z.; Xu, W.; Zhu, W.; Yang, Q.; Lei, X.; Liu, J.; Li, Y.; Sun, X.; Duan, X. Three-Dimensional NiFe Layered Double Hydroxide Film for High-Efficiency Oxygen Evolution Reaction. *Chem. Commun.* **2014**, *50* (49), 6479−6482.
(41) Gong, M.; Li, Y.; Wang, H.; Liang, Y.; Wu, J. Z.; Zhou, J.; Wang, J.; Regier, T.; Wei, F.; Dai, H. An Advanced Ni−Fe Layered Double Hydroxide Electrocatalyst for Water Oxidation. *J. Am. Chem. Soc.* **2013**, *135* (23), 8452−8455.
(42) Gong, M.; Dai, H. A Mini Review of NiFe-Based Materials as Highly Active Oxygen Evolution Reaction Electrocatalysts. *Nano Res.* **2015**, *8* (1), 23−39.
(43) Ma, W.; Ma, R.; Wang, C.; Liang, J.; Liu, X.; Zhou, K.; Sasaki, T. A Superlattice of Alternately Stacked Ni−Fe Hydroxide Nanosheets and Graphene for Efficient Splitting of Water. *ACS Nano* **2015**, *9* (2), 1977−1984.
(44) Pérez-Alonso, F. J.; Adán, C.; Rojas, S.; Peña, M. A.; Fierro, J. L. G. Ni/Fe Electrodes Prepared by Electrodeposition Method over Different Substrates for Oxygen Evolution Reaction in Alkaline Medium. *Int. J. Hydrogen Energy* **2014**, *39* (10), 5204−5212.
(45) Song, F.; Hu, X. Exfoliation of Layered Double Hydroxides for Enhanced Oxygen Evolution Catalysis. *Nat. Commun.* **2014**, *5*, 4477.
(46) Liang, H.; Meng, F.; Cabán-Acevedo, M.; Li, L.; Forticaux, A.; Xiu, L.; Wang, Z.; Jin, S. Hydrothermal Continuous Flow Synthesis and Exfoliation of NiCo Layered Double Hydroxide Nanosheets for Enhanced Oxygen Evolution Catalysis. *Nano Lett.* **2015**, *15* (2), 1421−1427.
(47) Costentin, C.; Saveant, J.-M. Cyclic Voltammetry Analysis of Electrocatalytic Films. *J. Phys. Chem. C* **2015**, *119* (22), 12174−12182.
(48) May, K. J.; Carlton, C. E.; Stoerzinger, K. A.; Risch, M.; Suntivich, J.; Lee, Y.-L.; Grimaud, A.; Shao-Horn, Y. Influence of Oxygen Evolution during Water Oxidation on the Surface of Perovskite Oxide Catalysts. *J. Phys. Chem. Lett.* **2012**, *3* (22), 3264−3270.
(49) Risch, M.; Grimaud, A.; May, K. J.; Stoerzinger, K. a.; Chen, T. J.; Mansour, A. N.; Shao-Horn, Y. Structural Changes of Cobalt-Based Perovskites upon Water Oxidation Investigated by EXAFS. *J. Phys. Chem. C* **2013**, *117* (17), 8628−8635.
(50) Grimaud, A.; May, K. J.; Carlton, C. E.; Lee, Y.-L.; Risch, M.; Hong, W. T.; Zhou, J.; Shao-Horn, Y. Double Perovskites as a Family of Highly Active Catalysts for Oxygen Evolution in Alkaline Solution. *Nat. Commun.* **2013**, *4*, 2439.
(51) Binninger, T.; Mohamed, R.; Waltar, K.; Fabbri, E.; Levecque, P.; Kötz, R.; Schmidt, T. J. Thermodynamic Explanation of the Universal Correlation between Oxygen Evolution Activity and Corrosion of Oxide Catalysts. *Sci. Rep.* **2015**, *5*, 12167.
(52) Doyle, R. L.; Godwin, I. J.; Brandon, M. P.; Lyons, M. E. G. Redox and Electrochemical Water Splitting Catalytic Properties of Hydrated Metal Oxide Modified Electrodes. *Phys. Chem. Chem. Phys.* **2013**, *15* (33), 13737−13783.
(53) Surendranath, Y.; Kanan, M. W.; Nocera, D. G. Mechanistic Studies of the Oxygen Evolution Reaction by a Cobalt-Phosphate Catalyst at Neutral pH. *J. Am. Chem. Soc.* **2010**, *132* (14), 16501−16509.
(54) Bediako, D. K.; Surendranath, Y.; Nocera, D. G. Mechanistic Studies of the Oxygen Evolution Reaction Mediated by a Nickel−Borate Thin Film Electrocatalyst. *J. Am. Chem. Soc.* **2013**, *135* (9), 3662−3674.
(55) Kanan, M. W.; Nocera, D. G. In Situ Formation of an Oxygen-Evolving Catalyst in Neutral Water Containing Phosphate and Co^{2+}. *Science* **2008**, *321* (5892), 1072−1075.
(56) Corrigan, D. A.; Bendert, R. M. Effect of Coprecipitated Metal Ions on the Electrochemistry of Nickel Hydroxide Thin Films: Cyclic Voltammetry in 1M KOH. *J. Electrochem. Soc.* **1989**, *136* (3), 723−728.

DOI: 10.1021/acs.chemmater.5b03148
Chem. Mater. 2015, 27, 7549−7558

(57) Merrill, M. D.; Dougherty, R. C. Metal Oxide Catalysts for the Evolution of O_2 from H_2O. *J. Phys. Chem. C* **2008**, *112* (10), 3655−3666.
(58) Burke, M. S.; Zou, S.; Enman, L. J.; Kellon, J. E.; Gabor, C. A.; Pledger, E.; Boettcher, S. W. Revised Oxygen Evolution Reaction Activity Trends for First-Row Transition Metal (Oxy)hydroxides in Alkaline Media. *J. Phys. Chem. Lett.* **2015**, *6*, 3737−3742.
(59) Trasatti, S.; Petrii, O. A. Real Surface Area Measurements in Electrochemistry. *J. Electroanal. Chem.* **1992**, *327* (1−2), 353−376.
(60) McCrory, C. C. L.; Jung, S.; Peters, J. C.; Jaramillo, T. F. Benchmarking Heterogeneous Electrocatalysts for the Oxygen Evolution Reaction. *J. Am. Chem. Soc.* **2013**, *135* (45), 16977−16987.
(61) Batchellor, A. S.; Boettcher, S. W. Pulse-Electrodeposited Ni-Fe (oxy)hydroxide Oxygen Evolution Electrocatalysts with High Geometric and Intrinsic Activities at Large Mass Loadings. *ACS Catal* **2015**, DOI: 10.1021/acscatal.5b01551.
(62) Corrigan, D. A.; Knight, S. L. Electrochemical and Spectroscopic Evidence on the Participation of Quadrivalent Nickel in the Nickel Hydroxide Redox Reaction. *J. Electrochem. Soc.* **1989**, *136* (3), 613−619.
(63) Barnard, R.; Randell, C. F.; Tye, F. L. Studies Concerning Charged Nickel Hydroxide Electrodes I. Measurement of Reversible Potentials. *J. Appl. Electrochem.* **1980**, *10* (1), 109−125.
(64) Klingan, K.; Ringleb, F.; Zaharieva, I.; Heidkamp, J.; Chernev, P.; Gonzalez-Flores, D.; Risch, M.; Fischer, A.; Dau, H. Water Oxidation by Amorphous Cobalt-Based Oxides: Volume Activity and Proton Transfer to Electrolyte Bases. *ChemSusChem* **2014**, *7* (5), 1301−1310.
(65) Louie, M. W.; Bell, A. T. An Investigation of Thin-Film Ni−Fe Oxide Catalysts for the Electrochemical Evolution of Oxygen. *J. Am. Chem. Soc.* **2013**, *135* (33), 12329−12337.
(66) Zou, S.; Burke, M. S.; Kast, M. G.; Fan, J.; Danilovic, N.; Boettcher, S. W. Fe (Oxy)hydroxide Oxygen Evolution Reaction Electrocatalysis: Intrinsic Activity and the Roles of Electrical Conductivity, Substrate, and Dissolution. *Chem. Mater.* **2015**, submitted.
(67) Klaus, S.; Cai, Y.; Louie, M. W.; Trotochaud, L.; Bell, A. T. Effects of Fe Electrolyte Impurities on $Ni(OH)_2$/NiOOH Structure and Oxygen Evolution Activity. *J. Phys. Chem. C* **2015**, *119* (13), 7243−7254.
(68) Friebel, D.; Louie, M. W.; Bajdich, M.; Sanwald, K. E.; Cai, Y.; Wise, A. M.; Cheng, M.-J.; Sokaras, D.; Weng, T.-C.; Alonso-Mori, R.; Davis, R. C.; Bargar, J. R.; Nørskov, J. K.; Nilsson, A.; Bell, A. T. Identification of Highly Active Fe Sites in (Ni,Fe)OOH for Electrocatalytic Water Splitting. *J. Am. Chem. Soc.* **2015**, *137* (3), 1305−1313.
(69) Xiao, C.; Lu, X.; Zhao, C. Unusual Synergistic Effects upon Incorporation of Fe and/or Ni into Mesoporous Co_3O_4 for Enhanced Oxygen Evolution. *Chem. Commun.* **2014**, *50* (70), 10122−10125.
(70) Iwakura, C.; Honji, A.; Tamura, H. The Anodic Evolution of Oxygen on Co_3O_4 Film Electrodes in Alkaline Solutions. *Electrochim. Acta* **1981**, *26* (9), 1319−1326.
(71) Grewe, T.; Deng, X.; Tüysüz, H. Influence of Fe Doping on Structure and Water Oxidation Activity of Nanocast Co_3O_4. *Chem. Mater.* **2014**, *26* (10), 3162−3168.
(72) Marini, S.; Salvi, P.; Nelli, P.; Pesenti, R.; Villa, M.; Kiros, Y. Oxygen Evolution in Alkali with Gas Diffusion Electrodes. *Int. J. Hydrogen Energy* **2013**, *38* (26), 11496−11506.
(73) Zhang, C.; Fagan, R. D.; Smith, R. D. L.; Moore, S. A.; Berlinguette, C. P.; Trudel, S. Mapping the Performance of Amorphous Ternary Metal Oxide Water Oxidation Catalysts Containing Aluminium. *J. Mater. Chem. A* **2015**, *3* (2), 756−761.
(74) Wu, M.-S. S.; Huang, K.-C. C. Enhanced Electrochemical Performance of Nickel Hydroxide Electrode with Monolayer Hollow Spheres Composed of Nanoflakes. *Int. J. Hydrogen Energy* **2011**, *36* (21), 13407−13413.
(75) Swierk, J. R.; Klaus, S.; Trotochaud, L.; Bell, A. T.; Tilley, T. D. Electrochemical Study of the Energetics of the Oxygen Evolution Reaction at Nickel Iron (Oxy)Hydroxide Catalysts. *J. Phys. Chem. C* **2015**, *119* (33), 19022−19029.
(76) Bocca, C.; Barbucci, A.; Delucchi, M.; Cerisola, G. Nickel−Cobalt Oxide-Coated Electrodes: Influence of the Preparation Technique on Oxygen Evolution Reaction (OER) in an Alkaline Solution. *Int. J. Hydrogen Energy* **1999**, *24* (1), 21−26.
(77) de Chialvo, M. R. G.; Chialvo, A. C. Oxygen Evolution Reaction on $Ni_xCo_{(3-x)}O_4$ Electrodes with Spinel Structure. *Electrochim. Acta* **1993**, *38* (15), 2247−2252.
(78) Dincă, M.; Surendranath, Y.; Nocera, D. G. Nickel-Borate Oxygen-Evolving Catalyst that Functions under Benign Conditions. *Proc. Natl. Acad. Sci. U. S. A.* **2010**, *107* (23), 10337−10341.
(79) Gao, M.; Sheng, W.; Zhuang, Z.; Fang, Q.; Gu, S.; Jiang, J.; Yan, Y. Efficient Water Oxidation Using Nanostructured α-Nickel-Hydroxide as an Electrocatalyst. *J. Am. Chem. Soc.* **2014**, *136* (19), 7077−7084.
(80) Hall, D. E. $Ni(OH)_2$-Impregnated Anodes for Alkaline Water Electrolysis. *J. Electrochem. Soc.* **1983**, *130* (2), 317−321.
(81) Klaus, S.; Louie, M. W.; Trotochaud, L.; Bell, A. T. Role of Catalyst Preparation on the Electrocatalytic Activity of $Ni_{1-x}Fe_xOOH$ for the Oxygen Evolution Reaction. *J. Phys. Chem. C* **2015**, *119* (32), 18303−18316.
(82) Kleinke, M. U.; Knoble, M.; Bonugli, L. O.; Teschke, O. Amorphous Alloys as Anodic and Cathodic Materials for Alkaline Water Electrolysis. *Int. J. Hydrogen Energy* **1997**, *22* (8), 759−762.
(83) Zhang, M.; de Respinis, M.; Frei, H. Time-Resolved Observations of Water Oxidation Intermediates on a Cobalt Oxide Nanoparticle Catalyst. *Nat. Chem.* **2014**, *6* (4), 362−367.
(84) Mueller, D. N.; Machala, M. L.; Bluhm, H.; Chueh, W. C. Redox Activity of Surface Oxygen Anions in Oxygen-Deficient Perovskite Oxides during Electrochemical Reactions. *Nat. Commun.* **2015**, *6*, 6097.
(85) Vovk, G.; Chen, X.; Mims, C. A. In Situ XPS Studies of Perovskite Oxide Surfaces under Electrochemical Polarization. *J. Phys. Chem. B* **2005**, *109* (6), 2445−2454.
(86) Sanchez Casalongue, H. G.; Ng, M. L.; Kaya, S.; Friebel, D.; Ogasawara, H.; Nilsson, A. In Situ Observation of Surface Species on Iridium Oxide Nanoparticles during the Oxygen Evolution Reaction. *Angew. Chem., Int. Ed.* **2014**, *53* (28), 7169−7172.
(87) Capehart, T. W.; Corrigan, D. A.; Conell, R. S.; Pandya, K. I.; Hoffman, R. W. In Situ Extended X-Ray Absorption Fine Structure Spectroscopy of Thin-Film Nickel Hydroxide Electrodes. *Appl. Phys. Lett.* **1991**, *58* (8), 865−867.
(88) Kim, S.; Tryk, D. A.; Antonio, M. R.; Carr, R.; Scherson, D. In Situ X-Ray Absorption Fine Structure Studies of Foreign Metal Ions in Nickel Hydrous Oxide Electrodes in Alkaline Electrolytes. *J. Phys. Chem.* **1994**, *98*, 10269−10276.
(89) Yeo, B. S.; Bell, A. T. In Situ Raman Study of Nickel Oxide and Gold-Supported Nickel Oxide Catalysts for the Electrochemical Evolution of Oxygen. *J. Phys. Chem. C* **2012**, *116* (15), 8394−8400.
(90) Rong, X.; Kolpak, A. M. Ab Initio Approach for Prediction of Oxide Surface Structure, Stoichiometry, and Electrocatalytic Activity in Aqueous Solution. *J. Phys. Chem. Lett.* **2015**, *6* (9), 1785−1789.
(91) Millet, P.; Grigoriev, S. *Renewable Hydrogen Technologies*; Gandía, L. M., Arzamendi, G., Diéguez, P. M., Eds.; Elsevier: 2013.
(92) Varcoe, J. R.; Atanassov, P.; Dekel, D. R.; Herring, A. M.; Hickner, M. A.; Kohl, P. A.; Kucernak, A. R.; Mustain, W. E.; Nijmeijer, K.; Scott, K.; Xu, T.; Zhuang, L. Anion-Exchange Membranes in Electrochemical Energy Systems. *Energy Environ. Sci.* **2014**, *7* (10), 3135−3191.
(93) Parrondo, J.; Arges, C. G.; Niedzwiecki, M.; Anderson, E. B.; Ayers, K. E.; Ramani, V. Degradation of Anion Exchange Membranes Used for Hydrogen Production by Ultrapure Water Electrolysis. *RSC Adv.* **2014**, *4* (19), 9875−9879.

DOI: 10.1021/acs.chemmater.5b03148
Chem. Mater. 2015, 27, 7549−7558